On Using the Anisotropy in the Thermal Resistance of Solid-Fluid Interfaces to More Effectively Cool Nano-electronics

Xiaoyu Wang¹, David Venerus¹, Ishwar K. Puri² and Sohail Murad^{1*}

Abstract

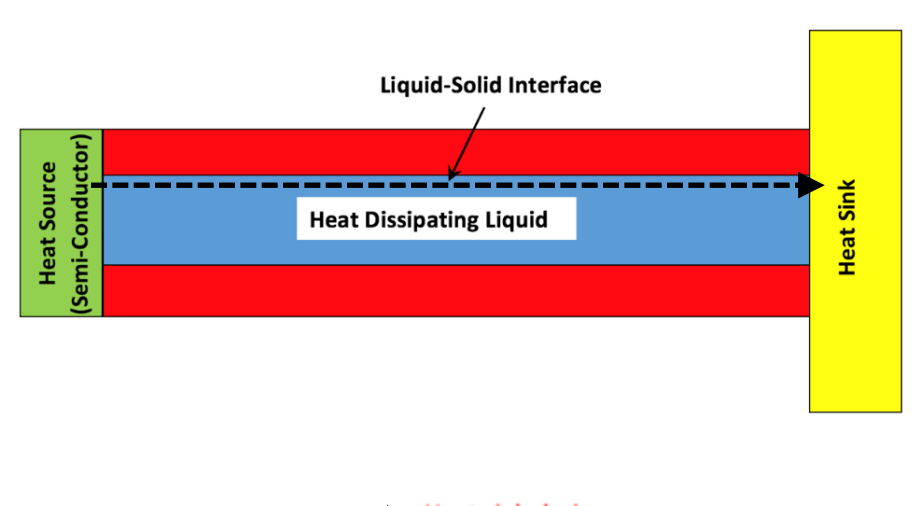
As power intensive electronic components are further miniaturized into nanodevices, their heat dissipation is a serious operational and safety concern. While nanochannels and nanofins are often used for facilitating heat dissipation, the liquid-solid interfaces that form (Kapitza resistance), become significant barriers to heat transfer. We demonstrate that the thermal resistance of these interfaces is strongly anisotropic. The resistance of an interface to heat transfer parallel to the interface (solid surface) is significantly smaller than the more well-known Kapitza resistance (associated with heat transfer across the interface —perpendicular to the solid surface) and is even lower than that of the bulk fluid. As a result, if devices are designed to dissipate heat parallel to an interface, heat dissipation can be significantly enhanced. Our studies are also able to explain the molecular basis of this observed anisotropy in interfacial resistance, which has hitherto remained unreported for solid-liquid interfaces.

¹ Department of Chemical and Biological Engineering, Illinois Institute of Technology, Chicago, USA

² Department of Mechanical Engineering, Department of Engineering Physics, and Department of Materials Science and Engineering, McMaster University, Hamilton, Ontario L8S 4L7, Canada

^{*} murad@iit.edu

The further miniaturization of high power consumption semiconductor devices is limited by the significant challenge posed by component overheating.[1] New strategies suggested for dissipating heat in nanoscale devices[2] include use of heat dissipating nanochannels and nanofins,[3, 4] where the interfacial thermal resistance across the solid-liquid interface plays an important role during heat dissipation.[5, 6, 7] The interface thickness can be significant fraction of the total system dimension, and the interfacial resistance can differ significantly from that of the bulk fluid as can be seen in Figure 1. While this interfacial resistance perpendicular to the solid-fluid interface, often referred to as Kapitza resistance R_{\perp} , has been the subject of numerous previous studies, in many devices the anisotropic surface resistance parallel to the surface R_{\parallel} also plays a significant role in heat dissipation. This anisotropy has not been previously examined for solid-fluid interfaces and is the main motivation for our study. For solid interfaces, such as silicon-films previous studies have reported anisotropy in the thermal resistance of the interface. [8]



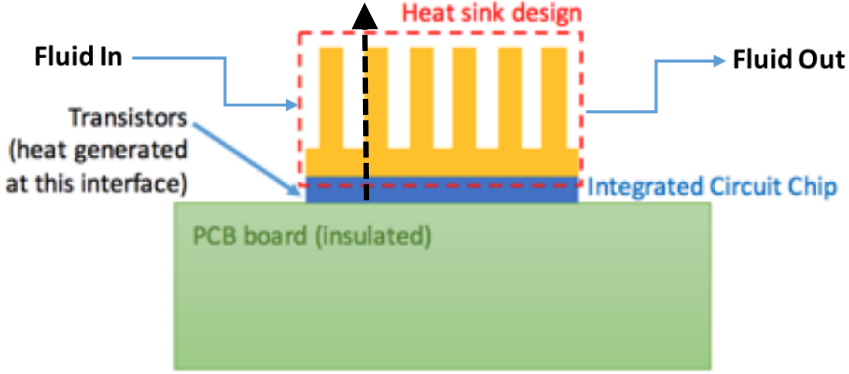


Figure 1: Conceptual design of a Nanochannels (top) and Nanofins (bottom) to facilitate heat dissipation from increasingly miniaturized semi-conductor chips. An example of the relative thickness of the interface compared to the total nano-channel thickness is indicated in the schematic for the nano-channel. Similar trends are prevalent in many such devices.

A nanoscale interface separating the two phases of a solid-solid, [8, 9] macromolecular, [10, 11, 12, 13] solid-liquid, [5, 14, 15, 16] or liquid-liquid [17] composite material generates a temperature discontinuity ΔT , which is the origin of R_{\perp} . [18, 19] For heat flow q^* across an interfacial area A, $R_{\perp} = A \cdot \Delta T / q^* \propto T^{-\alpha}$. [19, 20] When the interface thickness occupies a significant fraction of the overall dimension of a thermal system L (see Figure 1), for instance during axial heat dissipation in a nanochannel or photothermal heating, δ is a significant fraction of L. For such a case, since heat transfer can occur parallel to the interface as well as perpendicular to it, R_{\perp} alone cannot be used to adequately represent q^* , and R_{\parallel} must also be accounted for. Although the measurements are challenging, [21] R_{\perp} has been characterized both experimentally and through molecular simulations. Considering that similar measurements of heat transfer along, or parallel to, a nanoscale interface would be even more challenging, only a few studies have been reported for solid-solid interfaces, but none for solid-liquid values of R_{\parallel} .

We therefore design molecular dynamics (MD) simulations to investigate thermal transport both perpendicular and parallel to solid-liquid interface. In our investigations we have included three liquids (fluids) confined within copper walls. Of these liquids, water and methanol are polar, whereas benzene is nonpolar. Figure 2 presents a schematic of a 130.14 × 65.07 × 28.92 Å reservoir of x, y, z dimensions respectively that contains a liquid within solid walls. Yellow, blue and gray sections represent copper walls of 10.845 Å, 21.69 Å and 10.845 Å thicknesses, respectively. The yellow walls are maintained at higher temperatures than those shaded blue. By imposing periodic boundary conditions, in effect the two warmer yellow walls Λ_h constitute a single congruent wall of the same thickness as the cooler blue wall Λ_c . Liquid is confined within these walls with the result that the system includes several distinct solid-liquid stationary interfaces, which permit the examination of well-defined liquid density profiles.[22] This unique setup permits us to examine the thermal resistance of both the perpendicular and parallel interfaces simultaneously through a single simulation.

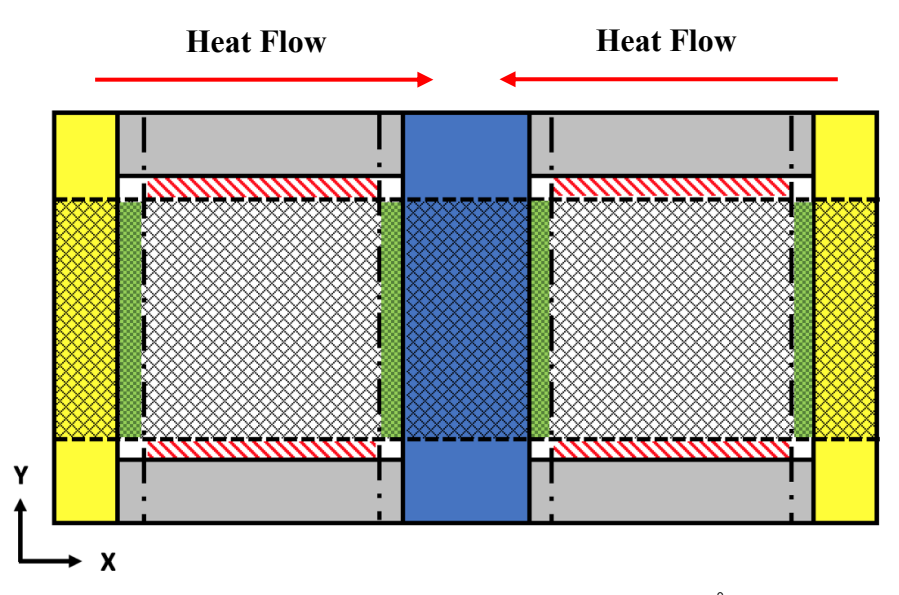


Figure 2: A Schematic (not to scale) of the $130.14 \times 65.07 \times 28.92$ Å simulation systems investigated containing liquid confined within solid walls. The yellow region indicates the hot copper wall (at temperature T_h) Λ_h ; blue the cold copper wall Λ_c (temperature T_c); unhatched gray Λ_a , copper wall sections where temperature is not controlled (copper walls of 10.845 Å, 21.69 Å and 10.845 Å thicknesses.) The Λ_h walls are at higher temperatures than Λ_c , resulting in heat transfer in the direction indicated (perpendicular to the green interface δ_L but parallel to the red interface δ_L that lies along the Λ_a). The gray hatched regions identify the "bulk", fluid region (away from the interfaces). The white regions at the intersection of the copper walls indicate "double" interfaces. This region, because of this added complexity, is not used in our interfacial thermal resistance calculations.

We focus on thermal transport parallel and perpendicular, respectively, to the red (δ_{\parallel}) and green (δ_{\perp}) interfaces of Fig. 2. The molar densities of the liquids allow us to fill the volume between the system walls with 3400 water, or 1500 methanol, or 800 benzene molecules. The copper walls (yellow, blue and grey) are constituted from 11,520 copper atoms. Heat transfer from the hot copper walls Λ_h to the cooler copper wall Λ_c occurs perpendicular to the green interfacial layer Λ_{\perp} , while it proceeds parallel to the red interfacial layer δ_{\parallel} along the gray wall Λ_a , the outside edges of which are adiabatic.

As indicated earlier, this arrangement allows us to simultaneously examine the thermal resistance perpendicular to, or across, δ_{\perp} and parallel to, or along, δ_{\parallel} . To obtain the thermal conductivity κ_{\perp} perpendicular to the interface, we monitor the heat added to Λ_h in the yellow hatched area of Fig. 2 and that removed from the corresponding blue hatched area for Λ_c . Using the Fourier law, the temperature decreases across δ_{\perp} and the surface area available for heat transfer enable calculation of κ_{\perp} . Similarly, the thermal conductivity κ_{\parallel} of δ_{\parallel} is obtained using the

temperature gradient along the interface, depicted by red diagonal lines in Fig. 2, and the heat input and removal from the corresponding sections of Λ_h and Λ_c . Since the system provides two independent measurements for the top and bottom sections in the x direction, the simulation error can also be estimated. Such a system setup and simulation method have been documented in our previous publications [5, 23] and proved effective in investigating solid-fluid, and solid-solid interfacial thermal resistances [24, 25, 26, 27] Other investigators have also recently used similar methods to investigate interfacial thermal resistance in a wide range of systems, including melting crystals and stacked thin films.[28, 29, 30]

For methanol and benzene, the Jorgensen United Atom OPLS force field [31, 32] is used to represent their potential models,

$$E_{\text{total}} = \sum_{\text{bonds}} K_b (r - r_{eq})^2 + \sum_{\text{angles}} K_\theta (\theta - \theta_{eq})^2 + \sum_{i < j} 4\varepsilon \left[\left(\frac{\sigma_{ij}}{r_{ij}} \right)^{12} - \left(\frac{\sigma_{ij}}{r_{ij}} \right)^6 \right] + \sum_{i < j} \frac{Cq_i q_j}{\varepsilon r_{ij}} \qquad for \ r_{ij} < r_c (12\text{Å})$$
(1)

The first three terms in Eq. (1) represent the intramolecular energies for forces associated with bonds, bond angles and dihedral angles, while the last two correspond to the dispersion and coulombic intermolecular energies. For water molecules a TIP3P potential model is employed [33], and for copper atoms the EAM model represents the force field. [34] The Lennard-Jones (LJ) 12-6 potential models short-range site-site interactions and cross terms were estimated using standard mixing rules. For the cross term between copper and liquid molecules, copper atoms are treated as LJ particles. [35] To determine long-range electrostatic forces and energies, a particle-particle particle-mesh solver [36] is used, which is computationally more efficient while being equally reliable as the traditional Ewald technique.

Use of the Packmol [37] open source software package provides the initial liquid-like random non-overlapping molecular configurations, which assist the system in more rapidly reaching steady state. [38, 39, 40] All simulations are performed with the LAMMPS simulation package with a time step of 1 femtosecond. [41] All atoms/molecules were initially assigned velocities corresponding to the desired temperatures with a Gaussian distribution to enable the system to reach its equilibrium/steady state faster. This system was studied in an NVE ensemble. A Langevin thermostat [42] which controls temperatures by modifying the forces is only applied to the atoms constituting the hot and cold regions of the copper walls. The thermostat applied to

the hot and cold walls is monitored to record the energy supplied or extracted to determine the heat flux needed in the thermal resistance calculations carried out. The fluid in the system was "equilibrated" at its average temperature, (average of the hot and cold walls temperatures), for 10 picoseconds followed by an additional simulation of 1 nanosecond to allow the system to approach steady state before any energies and temperatures are sampled. A final production run of 3 nanoseconds was carried out to sample the heat flux, density and temperature profiles within the system to obtain the properties reported. To ensure that the system had reached (approached) steady state, we compared results over the last 1 ns of the simulation with those over the last 2 and 3 ns and confirmed that the heat flux and temperature and density values had converged. As mentioned earlier our simulation set up provides us two sets of independent results that can also be used ensure that our simulations have converged. In addition, we did carry out additional simulations with different starting configurations to ensure no systematic errors in our simulations. A summary of the simulated cases is provided in Table 1. The interfacial thermal resistances (R) reported were estimated using the Fourier eqn $(R = A \cdot \Delta T / q)$, noting that $\kappa = 1/R$). For the perpendicular interfacial resistance, we obtained the heat removed added for the copper walls in the hatched yellow and blue areas and obtained the temperature gradient in the green interfacial region. For the parallel interfacial resistance, we once again obtained the heat added or removed in the hot (yellow unhatched) and cold (blue unhatched) walls in the region aligned with the red hatched interfacial regions, where we obtained the temperature gradient. The results are shown in Figures 3-6.

Table 1. Ratio of the parallel interfacial thermal conductivity κ_{\parallel} along the red interface δ_{\parallel} (cf. Fig. 2) to the perpendicular conductivity κ_{\perp} across the green interface δ_{\perp} , ratio of κ_{\parallel} to the bulk thermal conductivity κ_b . The thickness of the green and red interfaces was statistically equal (cf. Fig. 2) for different cases so δ values represent both interfaces.

Case	Holt-cold wall temperatures, K	Fluid	Wall	δ/Å	$\kappa_{ }/\kappa_{\perp}$	$\kappa_{ }/\kappa_{b}$
1	600-300	Water	Neutral	5.4	11.65±2.23	2.26±0.07
2	550-350	Water	Neutral	7.2	6.12±1.26	1.48±0.04
3	600-300	Water	Charged	9.0	4.71±0.72	1.47±0.05
4	600-300	Methanol	Neutral	9.0	12.71±1.62	6.05±0.35
5	500-300	Benzene	Neutral	9.0	5.11±0.98	2.28±0.36
6	450-350	Benzene	Neutral	9.0	4.71±0.82	2.28±0.28

For Cases 1 and 2, the reservoir contains water between inert walls with hot-cold temperatures being 600-300K and 550-350K, respectively, i.e., the temperature differences ΔT are 300 and 200K. Case 3 corresponds to ΔT for Case 1 but with reservoir walls that are charged and made hydrophilic by introducing small 0.1e negative charges and corresponding positive charges on alternating copper wall atoms. Temperature contours for all three cases, shown in Fig. 3, reveal quasi-uniform temperature stratification along the direction of heat transfer in the large central bulk of the reservoir. Due to the local Kapitza resistances that form along the hot and cold walls, the temperatures change rapidly across their corresponding $\delta_{\rm L}$ interfaces. Since copper is a better thermal conductor than water, Δ_a more effectively cools and heats the Δ_h and Δ_c than water. Consequently, the temperature stratifications along Δ_a , therefore within the $\delta_{\rm H}$, differ from those in the central bulk of the system where the temperature profile from the hot to the cold side is steeper.

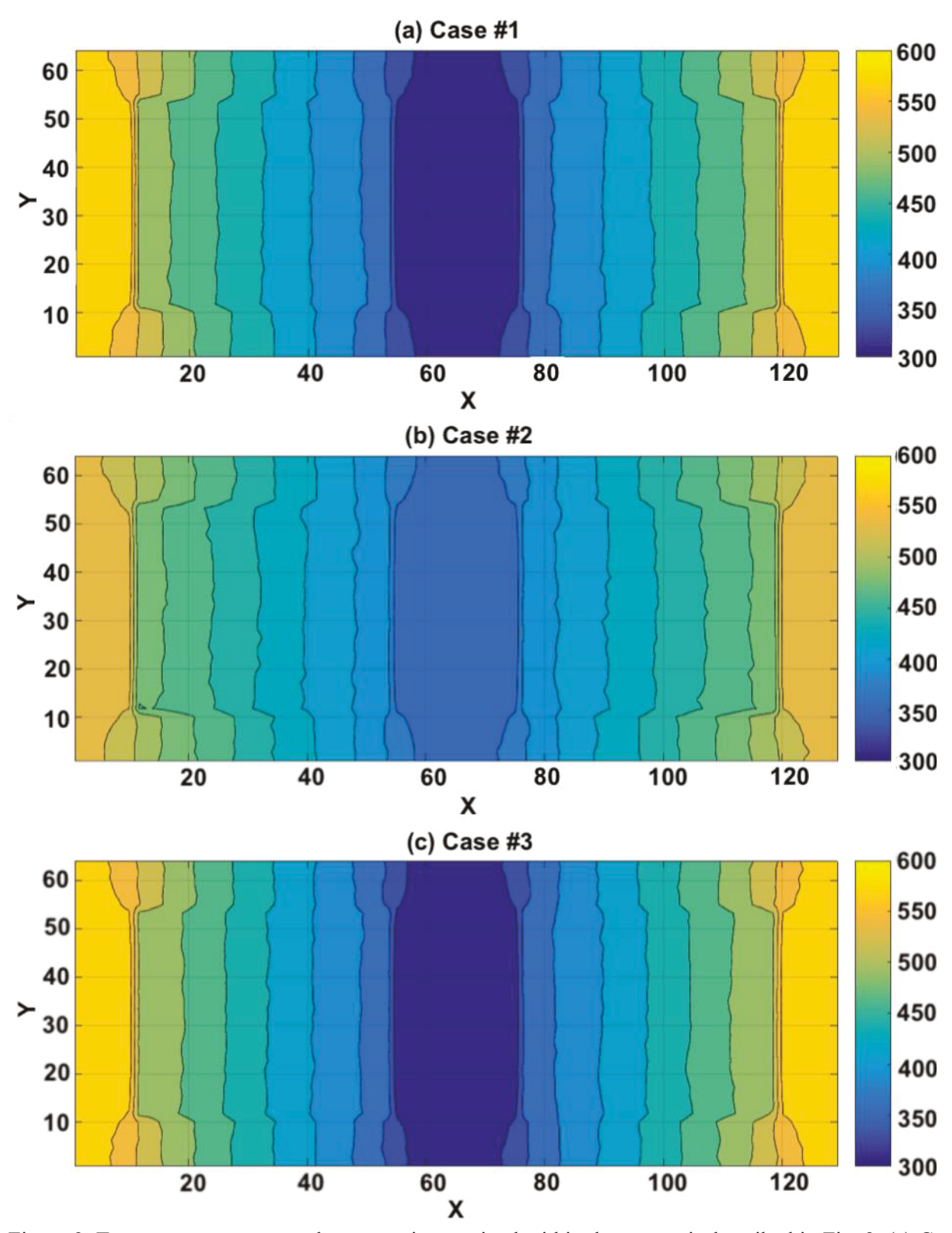


Figure 3. Temperature contours when water is contained within the reservoir described in Fig. 2. (a) Case 1when the reservoir walls are inert and boundary temperatures at Λ_h and Λ_c of 600K and 300K. (b) Case 2 with inert walls and 550K and 350K boundary temperatures. (c) Case 3 with charged walls and 600K and 300K boundary temperatures.

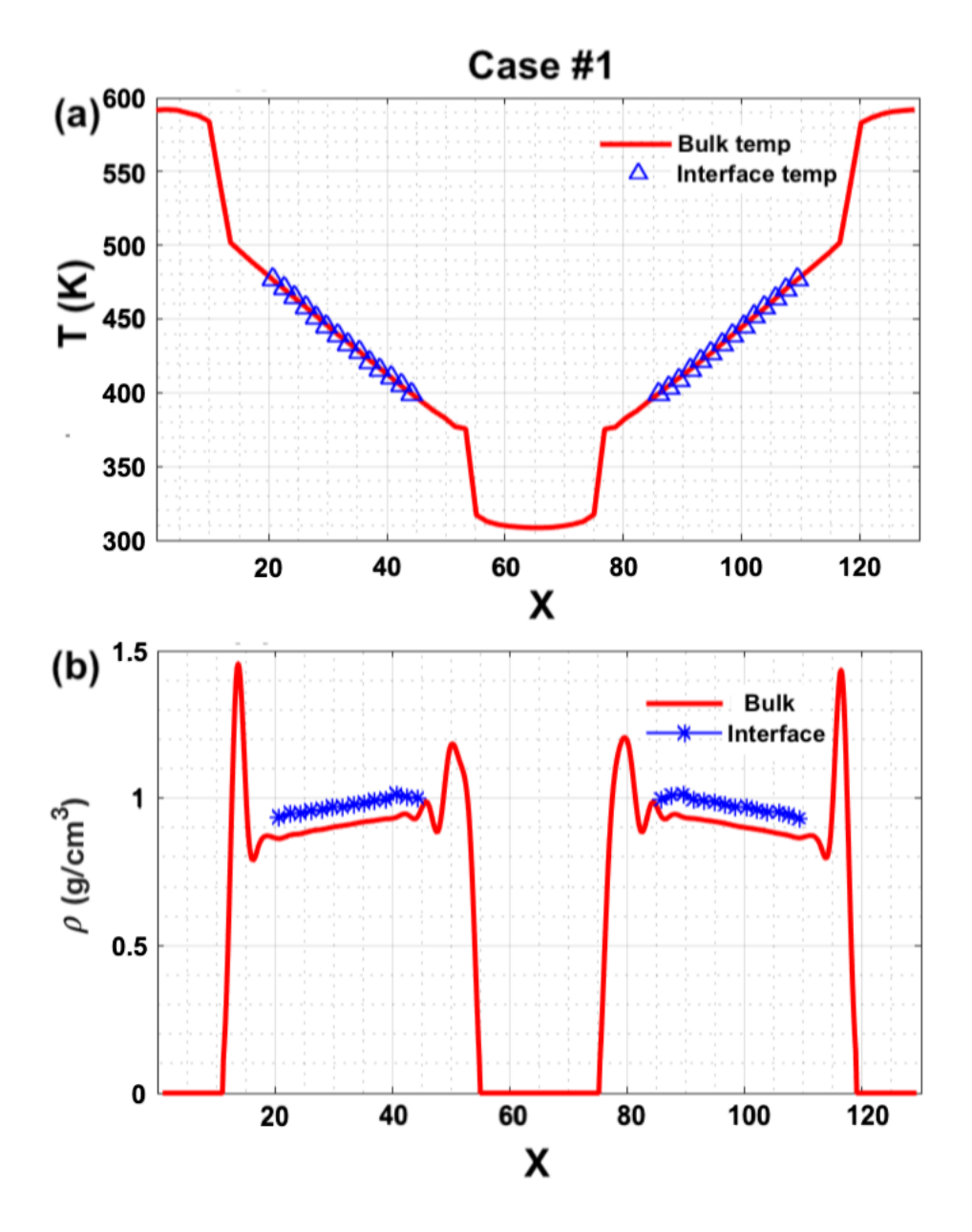


Figure 4. Temperature (a) and density profiles (b) for the bulk fluid (grey hatched region in Figure 2) and the interfacial layer (red hatched region). These results are for case 1 in Table 1, where the hot wall is at 600 K and cold wall at 300 K and the fluid being investigated is water.

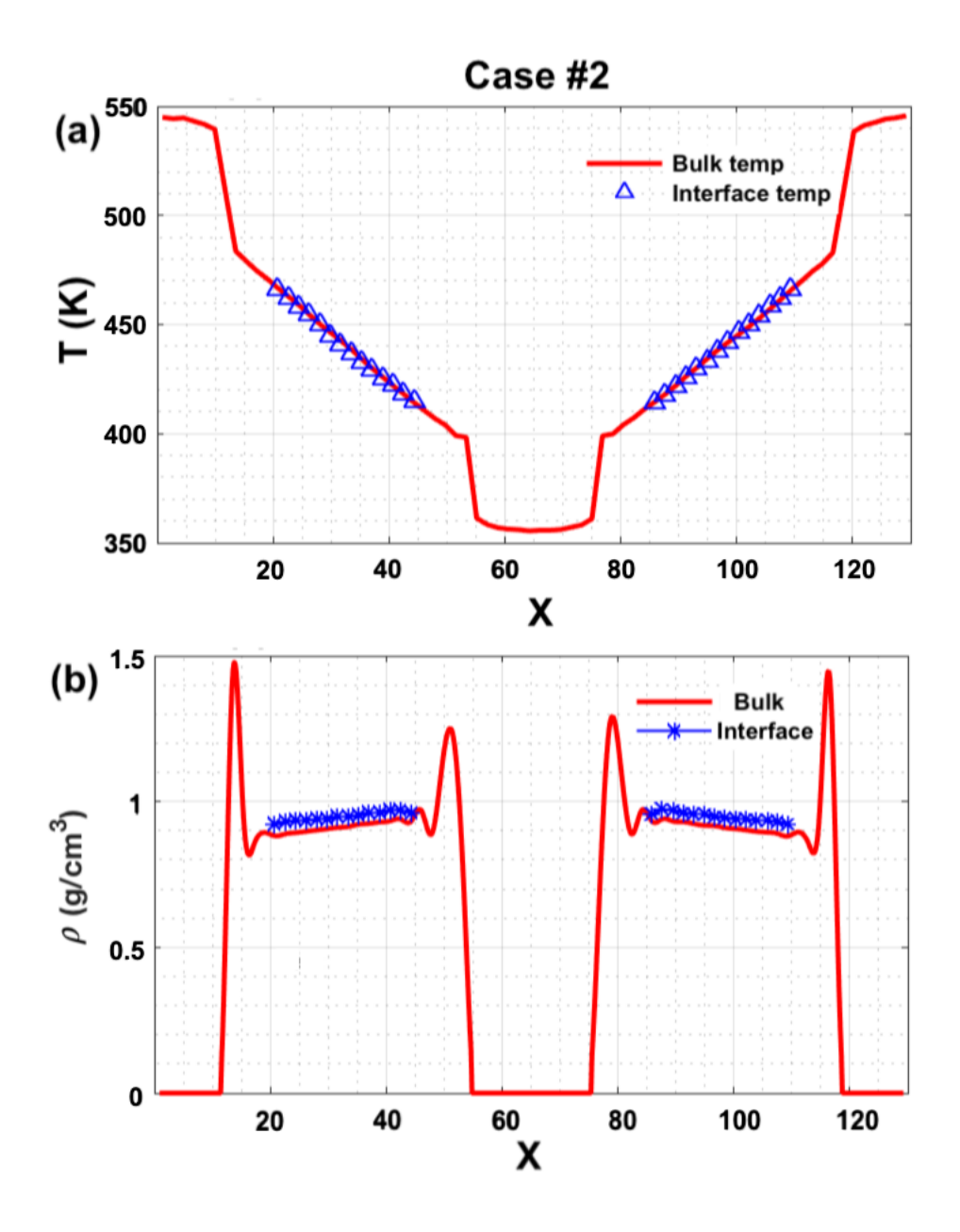


Figure 5. Temperature (a) and density profiles (b) for the bulk fluid (grey hatched region in Figure 2) and the interfacial layer (red hatched region). These results are for case 2 in Table 1, where the hot wall is at 550 K and cold wall at 350 K and the fluid being investigated is water.

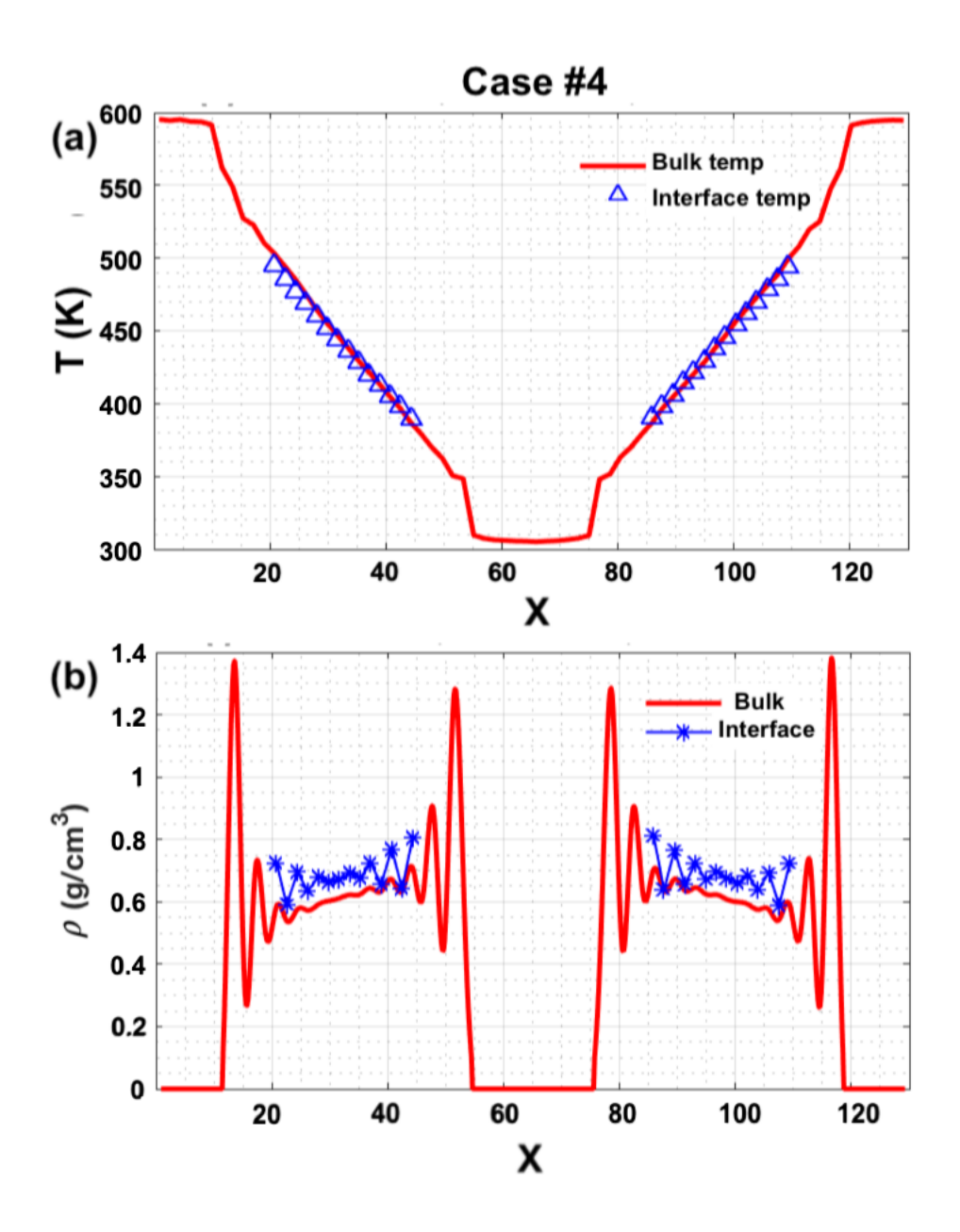


Figure 6. Temperature (a) and density profiles (b) for the bulk fluid (grey hatched region in Figure 2) and the interfacial layer (red hatched region). These results are for case 4 in Table 1, where the hot wall is at 600 K and cold wall at 300 K and the fluid being investigated is methanol.

Figures 4- 6 (a) present the water temperature profiles in δ_{\parallel} (red hatched ares) and the bulk fluid in the respective grey hatched areas of figure 1 for Cases 1, 2 and 4 of Table 1, while figure 4-6 (b)s show density profiles for those areas. In Figure 4(a), it can be seen that the temperature profiles in the interface layer and bulk fluid are almost identical. The simulation system was designed for negligible heat transfer along the y direction along the Λ_a grey walls. Our results confirm that this

was the case. In accordance with our previous observations, the density profile of Fig. 4(b) shows evidence of liquid stratification into distinct layers near the walls, i.e., in both hot and cold δ_{\perp} that are adjacent to Λ_h and Λ_c . [43, 44] While this stratification also occurs along δ_{\parallel} , heat transfer parallel to Λ_a occurs along strata where the water density is higher, enhancing overall heat transfer along that interface, as discussed below. Consequently, $\kappa_{||} > \kappa_b$ (and κ_{\perp}). The reported density of "bulk" region refers to the average density of the entire "bulk" region, whose density obviously varies because of the temperature gradient in our system.. The density variations in the x direction observed in figure 4(b) are largely due to the large temperature gradient in the system in the x direction. The adsorption layers on the hot side are closer to the walls because of larger kinetic energy of the molecules. We believe because of this closer proximity to the walls, the peak heights of the adsorption layer are larger. On the cold wall side, the adsorption layer is wider than that on hot wall side. This can be explained as water can more easily associate at lower temperatures, while near the hot wall side, higher kinetic energy will inhibit such associations. Figures 5(a) and (b) show corresponding results for different temperatures, which are qualitatively similar to figure 4(a) and (b). Results for methanol are shown in Figure 6(a) and (b). Since methanol is less polar (dipole moment of 1.7 D vs. 1.85 D for water) and also more mobile than water, its density profile is less uniform, which is evident from Fig. 6(b). Another interesting observation from figure 6(b) is that methanol density profile has larger fluctuations. Methanol does hydrogen bond but they are weaker than those of water. We believe this leads to larger fluctuations than those found in water. We similarly see larger fluctuations in hydrocarbons too which do not associate as well.

We believe this to be the first study to unambiguously demonstrate anisotropy in the thermal conductivities of solid-liquid interfaces (anisotropy in solid-solid interfaces has been reported previously) in a confined and enclosed nanochannels (Table 1 shows that for all cases, $\kappa_{\parallel} > (\kappa_{\perp} \text{ or } \kappa_b)$. This is readily understood from Figs. 2 and 4(b) by examining the two green δ_{\perp} interfaces adjacent to Λ_h and Λ_c . For heat transfer to occur across δ_{\perp} against the thermal gradient as prescribed by the Fourier Law, the implication of Fig. 4(b) is that phonons moving from Λ_h to Λ_c are first transported across a region of low liquid density adjacent to the solid surface, then across the higher density first adsorption peak, and again through another density trough. The presence of these intervening vacancies reduces overall heat transfer across δ_{\perp} significantly. [44]

The enhancement of thermal conductivity reported here has also been reported in a recent paper by Han et al. who reported a decrease in the thermal resistance of the interface, when the interfacial density increased because of higher system pressure. [45] In contrast, along $\delta_{||}$, although heat transfer along low density regions is again diminished, overall thermal transport occurs far more effectively along stratified higher density layers. Since heat transfer occurs more effectively through $\delta_{||}$ than in the bulk fluid, nanoscale strategies should consider dissipating heat along such interfaces rather than in the bulk.

Values of the water-copper interfacial thickness δ are provided in Table 1 for various cases. As noted earlier, δ_1 and δ_1 are found to be of approximately equal thickness. The thickness of the interfaces results primarily from the nature of the solid-fluid adsorption. The interface is defined here as the two adsorption layers adjacent to the solid surface. Since the fluid and the wall are identical for both the parallel and perpendicular interphases, it is not surprising that the thicknesses are also similar. With water as heat transfer fluid, increasing ΔT across the reservoirs decreases δ . As has been found in adsorption studies too, decreasing ΔT increases the adsorption layer thickness from 5.4 Å for Case 1 to 7.2 Å for Case 2. When the wall is charged it becomes more hydrophilic, which also increases adsorption. Hence, δ thickens for Case 3 to 9 Å, or about three molecular layers. From cases 1 to 3, we observe a decrease in the anisotropy in thermal conductivity when the thickness of solid-liquid interface increases, as does its value w.r.t. the bulk thermal conductivity of the fluid. For methanol (Case 4), the 9 Å interfacial layer is thicker than for water, since as Fig. 6(b) shows the methanol interface contains two adsorption layers. In case of benzene (Cases 5 and 6), δ is again 9 Å for a single adsorption layer because of the larger size of the benzene molecule.

For water, both $\kappa_{||}/\kappa_{\perp}$ and $\kappa_{||}/\kappa_b$ increase with ΔT (Cases 1 and 2 in Table 1). Our results show that as the interface thickness decreases from Case 1 to 2, the overall interface density in fact increases, as is evident in Figs .4(b) and 5(b). While this density increase has a significant influence on $\kappa_{||}$ its effect κ_{\perp} or on κ_b is far smaller, which explains the observed behavior. The inclusion of charges on the wall, making it hydrophilic, has an effect similar to that of lowering ΔT so that the results are qualitatively similar to Case 2. For nonpolar benzene, changes in ΔT (Cases 5 and 6) do not have a significant effect on the interface thickness and, as a result $\kappa_{||}/\kappa_{\perp}$ and $\kappa_{||}/\kappa_b$ do not change significantly. For all six Cases 1-6 in Table 1, heat transfer along $\delta_{||}$ is augmented by at

least $\approx 50\%$ compared to that through the bulk fluid. With methanol (Case 4) this enhancement is six times so that the design also offers a tunable strategy to alter $\kappa_{\parallel}/\kappa_b$ by changing the working fluid. Overall, Table 1 shows how $\kappa_{\parallel}/\kappa_{\perp}$ can be five to twelvefold larger making a strong case to design nanochannels to dissipate heat parallel to an interface rather than perpendicular to it, which is often the case in current heat dissipation devices.

In summary, the results demonstrate the efficacy of a strategy to enhance heat dissipation in high power consuming nanodevices more effectively than in current designs of many heat dissipation devices. Preliminary studies reveal a similar anisotropy in the thermal conductivity of liquid-liquid interfaces, indicating that this phenomenon is likely universal.

Acknowledgement: This research was supported by a grant from the National Science Foundation (CBET 1545560) and a Discovery Grant from the Natural Sciences and Engineering Research Council of Canada (RGPIN-2014-04066).

References

- 1. Moore AL, Shi L. Emerging challenges and materials for thermal management of electronics. Materials Today. 2014;17:163-74.
- 2. Hansson J, Nilsson TM, Ye L, Liu J. Novel nanostructured thermal interface materials: a review. International Materials Reviews. 2018;63:22-45.
- 3. Marable DC, Shin S, Nobakht AY. Investigation into the microscopic mechanisms influencing convective heat transfer of water flow in graphene nanochannels. International Journal of Heat and Mass Transfer. 2017;109:28-39.
- 4. Vo TQ, Kim B. Transport phenomena of water in molecular fluidic channels. Scientific Reports. 2016;6:33881.
- 5. Murad S, Puri IK. Thermal transport across nanoscale solid-fluid interfaces. Applied Physics Letters. 2008;92:133105.
- 6. Murad S, Puri IK. Molecular simulation of thermal transport across hydrophilic interfaces. Chemical Physics Letters. 2008;467:110-3.

- 7. Murad S, Puri IK. Thermal transport through a fluid-solid interface. Chemical Physics Letters. 2009;476:267-70.
- 8. Murad S, Puri IK. Thermal transport through superlattice solid-solid interfaces. Applied Physics Letters. 2009;95:051907.
- 9. Chang CW, Okawa D, Majumdar A, Zettl A. Solid-state thermal rectifier. Science. 2006;314:1121-4. Epub 2006/11/18.
- 10. Pal S, Balasubramanian G, Puri IK. Reducing thermal transport in electrically conducting polymers: Effects of ordered mixing of polymer chains. Applied Physics Letters. 2013;102:023109.
- 11. Murad S, Puri IK. Understanding unusual thermal transport behavior in soft materials under mechanical strain—A molecular dynamics study. Chemical Physics Letters. 2015;626:102-5.
- 12. Zhao B, Oroskar PA, Wang X, House D, Oroskar A, Oroskar A, Jameson C, Murad S. The Composition of the Mobile Phase Affects the Dynamic Chiral Recognition of Drug Molecules by the Chiral Stationary Phase. Langmuir. 2017;33:11246-56.
- 13. Xiaoyu Wang, David W. House, Priyanka A. Oroskar, Anil Oroskar, Asha Oroskar, Cynthia J. Jameson, Murad S. Molecular Dynamics Simulations of the Chiral Recognition Mechanism for a Polysaccharide Chiral Stationary Phase in Enantiomeric Chromatographic Separations. Molecular Physics. 2019. In press. DOI: https://doi.org/10.1080/00268976.2019.1647360
- 14. Hu M, Goicochea JV, Michel B, Poulikakos D. Thermal rectification at water/functionalized silica interfaces. Applied Physics Letters. 2009;95:151903.
- 15. Murad S, Puri IK. Thermal rectification in a fluid reservoir. Applied Physics Letters. 2012;100:121901--5.
- 16. Xue L, Keblinski P, Phillpot S, Choi S-S, Eastman J. Two regimes of thermal resistance at a liquid–solid interface. The Journal of Chemical Physics. 2003;118:337-9.
- 17. Murad S, Puri IK. Achieving thermal rectification in designed liquid-liquid systems. Applied Physics Letters. 2016;108:134101.
- 18. Kapitza PL. The Study of Heat Transfer in Helium II. Journal of Physics, USSR. 1941;4:181.

- 19. Pollack GL. Kapitza Resistance. Reviews of Modern Physics. 1969;41:48-81.
- 20. Murad S, Puri IK. Thermal transport across nanoscale solid-fluid interfaces. Applied Physics Letters. 2008;92:133105.
- 21. Zhao D, Qian X, Gu X, Jajja SA, Yang R. Measurement techniques for thermal conductivity and interfacial thermal conductance of bulk and thin film materials. Journal of Electronic Packaging. 2016;138:040802.
- 22. Wang X, Gu X, Murad S. Molecular dynamics simulations of liquid-liquid phase equilibrium of ternary methanol/water/hydrocarbon mixtures. Fluid Phase Equilibria. 2017.
- 23. Hinkle K, Wang X, Gu X, Jameson C, Murad S. Computational Molecular Modeling of Transport Processes in Nanoporous Membranes. Processes. 2018;6:124.
- 24. Kim BH, Beskok A, Cagin T. Molecular dynamics simulations of thermal resistance at the liquid-solid interface. The Journal of Chemical Physics. 2008;129:174701.
- 25. Barisik M, Beskok A. Temperature dependence of thermal resistance at the water/silicon interface. International Journal of Thermal Sciences. 2014;77:47-54.
- 26. Amani A, Karimian SMH, Seyednia M. A molecular dynamics simulation on the effect of different parameters on thermal resistance of graphene-argon interface. Molecular Simulation. 2017;43:276-83.
- 27. Pham AT, Barisik M, Kim B. Interfacial thermal resistance between the graphene-coated copper and liquid water. International Journal of Heat and Mass Transfer. 2016;97:422-31.
- 28. Liang Z, Keblinski P. Finite-size effects on molecular dynamics interfacial thermal-resistance predictions. Physical Review B. 2014;90:075411.
- 29. Liang Z, Sasikumar K, Keblinski P. Thermal Transport across a Substrate--Thin-Film Interface: Effects of Film Thickness and Surface Roughness. Physical Review Letters. 2014;113:065901.
- 30. Vo TQ, Kim B. Physical origins of temperature continuity at an interface between a crystal and its melt. The Journal of Chemical Physics. 2018;148:034703.
- 31. Jorgensen WL, Madura JD, Swenson CJ. Optimized intermolecular potential functions for liquid hydrocarbons. Journal of the American Chemical Society. 1984;106:6638-46.

- 32. Jorgensen WL. Optimized intermolecular potential functions for liquid alcohols. Journal of Physicsl Chemistry. 1986;90:1276-84.
- 33. Jorgensen WL, Chandrasekhar J, Madura JD, Impey RW, Klein ML. Comparison of simple potential functions for simulating liquid water. The Journal of chemical physics. 1983;79:926-35.
- 34. Foiles S, Baskes M, Daw MS. Embedded-atom-method functions for the fcc metals Cu, Ag, Au, Ni, Pd, Pt, and their alloys. Physical review B. 1986;33:7983.
- 35. Heinz H, Vaia R, Farmer B, Naik R. Accurate simulation of surfaces and interfaces of face-centered cubic metals using 12–6 and 9–6 Lennard-Jones potentials. The Journal of Physical Chemistry C. 2008;112:17281-90.
- 36. Hockney RW, Eastwood JW. Computer simulation using particles: crc Press; 1988.
- 37. Martínez L, Andrade R, Birgin EG, Martínez JM. PACKMOL: a package for building initial configurations for molecular dynamics simulations. Journal of computational chemistry. 2009;30:2157-64.
- 38. Qu F, Shi R, Peng L, Zhang Y, Gu X, Wang X, Murad S. Understanding the effect of zeolite crystal expansion/contraction on separation performance of NaA zeolite membrane: A combined experimental and molecular simulation study. Journal of Membrane Science. 2017;539:14-23.
- 39. Chen C, Cheng Y, Peng L, Zhang C, Wu Z, Gu X, Wang X, Murad S. Fabrication and stability exploration of hollow fiber mordenite zeolite membranes for isopropanol/water mixture separation. Microporous and Mesoporous Materials. 2019;274:347-55.
- 40. Wang X, Zhang Y, Wang X, Andres-Garcia E, Du P, Giordano L, Wang L, Hong Z, Gu X, Murad S, Kapteijn F. Xenon Recovery by DD3R Zeolite Membranes: Application in Anaesthetics. Angewandte Chemie. In press. DOI: https://doi.org/10.1002/ange.201909544
- 41. Plimpton S. Fast parallel algorithms for short-range molecular dynamics. Journal of computational physics. 1995;117:1-19.
- 42. Schneider T, Stoll E. Molecular-dynamics study of a three-dimensional one-component model for distortive phase transitions. Physical Review B. 1978;17:1302.

- 43. Banerjee S, Murad S, Puri IK. Preferential ion and water intake using charged carbon nanotubes. Chemical Physics Letters. 2007;434:292-6.
- 44. Balasubramanian G, Banerjee S, Puri IK. Unsteady nanoscale thermal transport across a solid-fluid interface. Journal of Applied Physics. 2008;104:064306.
- 45. Han H, Mérabia S, Mul er-Plathe F. Thermal Transport at Solid-Liquid Interfaces: High Pressure Facilitates Heat Flow through Nonlocal Liquid Structuring. Journal of Physical Chemistry Letter. 2017;8:1946-51.